

Progress of Beam-Beam Compensation Schemes

F. Zimmermann and U. Dorda, CERN, Geneva, Switzerland

Abstract

We review wire-based beam-beam compensation experiments in the SPS, prospects of wire-compensation studies at RHIC, exploratory ideas for future pulsed wire devices, simulations of LHC wire compensation, and requirements for LHC crab cavities.

1 NEED FOR BEAM-BEAM COMPENSATION

The nominal LHC parameters [1] are already challenging: The geometric luminosity loss from the crossing angle amounts to almost 20% and, in tracking studies, chaotic particle trajectories are found at amplitudes of $4-6\sigma$ in the presence of long-range beam-beam collisions [2, 3].

For an LHC upgrade, we likely increase the number of bunches or reduce β^* . Without any compensation larger crossing angles would then be required in order to mitigate the long-range beam-beam effects, but the resulting geometric luminosity loss would become unacceptable. This is illustrated in Fig. 1, which shows the geometric reduction factor

$$R_{\Theta} = \frac{1}{\sqrt{1 + \Theta^2}}, \quad (1)$$

as a function of the Piwinski angle

$$\Theta \equiv \frac{\theta_c \sigma_z}{2\sigma_x^*}. \quad (2)$$

The nominal LHC parameters correspond to a Piwinski angle of $\Theta = 0.65$ and a reduction factor $R_{\Theta} = 0.84$.

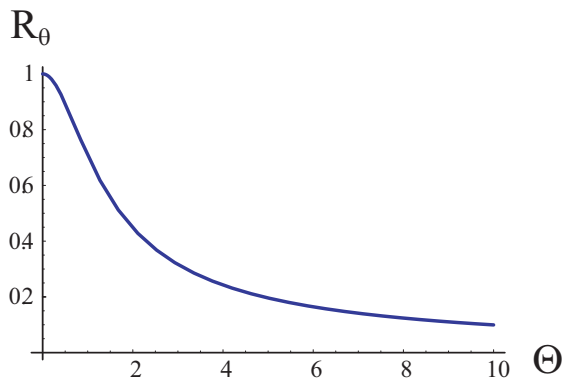


Figure 1: Geometric luminosity reduction factor R_{Θ} as a function of the Piwinski angle $\Theta \equiv \theta_c \sigma_z / (2\sigma_x^*)$.

Table 1 compares the Piwinski angles and luminosity reduction factors for lepton colliders and one hadron collider,

RHIC, with those for the nominal and ultimate LHC. The largest Piwinski angle is realized at KEKB, corresponding to 20% geometric luminosity loss. The beams in RHIC are thought to collide with a crossing angle of ± 0.5 mrad, with only a small effect on the luminosity. The LHC will be the first hadron collider with a design Piwinski parameter that is not negligible, and indeed close to the KEKB one.

Table 1: Piwinski angles and geometric luminosity reduction factors for various ring colliders

colliders	σ_z [mm]	σ_x^* [μm]	θ_c [mrad]	Θ $= \frac{\theta_c \sigma_z}{2\sigma_x^*}$	R_{Θ}
DORIS-1	10	230	24	0.52	0.89
DAFNE	18	700	30	0.39	0.93
	-40			-0.86	-0.76
KEKB	7	103	22	0.75	0.8
RHIC	140	177	± 0.5	0.20	0.98
nominal LHC	75.5	16.6	0.285	0.65	0.84
ultimate LHC	75.5	16.6	0.315	0.72	0.81

Simulations and experimental studies on the impact of a crossing angle were performed at both hadron and lepton colliders.

Strong-strong simulations predict an increase in the KEKB beam-beam tune shift limit by a factor 2–3 for head-on collisions compared with the present crossing angle [4]. This predicted performance enhancement constitutes the primary motivation for installing crab cavities in KEKB. The same simulations correctly predict the present KEKB performance.

RHIC operates with crossing angles of ± 0.5 mrad due to limited BPM resolution and diurnal orbit motion. Performance of proton stores is very irreproducible and frequently occurring lifetime problems could be related to the crossing angle, but this is not definitively proven [5].

The TEVATRON controls the crossing angle to better than $10 \mu\text{rad}$, and for angles of $10-20 \mu\text{rad}$ no lifetime degradation is seen [6].

The only controlled experiment of the crossing angle effect in a hadron collider was performed at the CERN SPS in 1991 [7]. This experiment showed no reduction of the beam lifetime for Piwinski angles up to $\Theta \geq 0.7$. Some experimental results are reproduced in Fig. 2.

To boost the LHC performance further various approaches have been proposed:

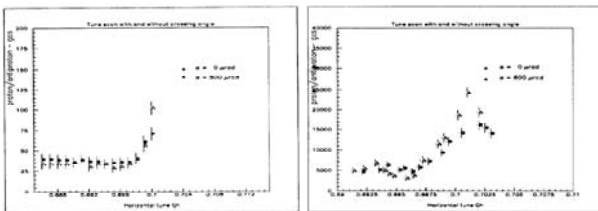


Figure 2: Beam lifetime signal in the SPS collider measured as a function of the horizontal tune, comparing scans for zero crossing angles with ones corresponding to a Pi-winski angle $\Theta = 0.45$ (left) or $\Theta \geq 0.70$ (right) [7].

- increase the crossing angle and reducing the bunch length (higher frequency rf, e.g., 1.2 GHz, & reduced longitudinal emittance [8, 9]);
- reducing the crossing angle and applying wire compensation [10, 11];
- using crab cavities, which allow for a large crossing angle without luminosity loss [12, 13, 14];
- colliding long intense bunches with a large crossing angle [15].

The baseline upgrade parameters, invoking either shorter or longer bunches [16], are listed in Table 2. Beam-beam compensation with wires or crab cavities would change the optimum beam parameters and could greatly affect the layout of the interaction region. The more-bunches option in the table already assumes a partial compensation of long-range beam-beam effects.

Without compensation, the minimum crossing angle imposed by the long-range beam-beam interaction is [16, 2, 17]

$$\theta_c \geq \sqrt{\frac{\epsilon}{\beta^*}} \left(\frac{d_{da}}{\sigma} + 3 \sqrt{\frac{k_{par}}{2 \times 32} \frac{N_b}{1.15 \times 10^{11}} \frac{3.75 \mu\text{m}}{\gamma \epsilon}} \right), \quad (3)$$

where d_{da}/σ denotes the dynamic aperture in units of the rms beam size and k_{par} the total number of long-range collisions at the two main interaction points. Equation (3) represents a scaling law first found by Irwin [18] with numerical values inferred from the simulations of [2]. Other simulations indicate the existence of a threshold, i.e., a few long-range encounters may have no effect on the dynamic aperture [17].

We assume that a dynamic aperture of $5-6\sigma$ is needed. Since the wire compensation is not efficient within 2σ from the center of the opposing beam, the minimum crossing angle achieved with a wire compensator is

$$\theta_{c,comp.} \geq 8 \sqrt{\frac{\epsilon}{\beta^*}}, \quad (4)$$

independent of beam current. Or in other words, a wire compensator reveals its strength for increasing bunch

charges and greater number of bunches, but it is less effective when the IP beta functions are reduced.

2 WIRE COMPENSATION

2.1 SPS Studies

Two beam-beam wire-compensator prototypes have been installed in the CERN SPS. Figure 3 shows one of two units from the second generation device. This compensator is equipped with three wires, which are separated from the beam vertically, horizontally, and at 45 degrees, respectively. It can be moved in the vertical direction over a range of 5 mm, via a remote control from the accelerator control room.

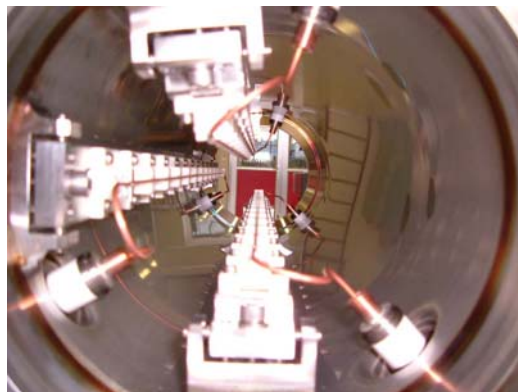


Figure 3: Photo of the second-generation 'BBLR' in the CERN SPS (G. Burtin, J. Camas, J.-P. Koutchouk, et al.)

By exciting a single compensator, we can model the effect of the uncompensated long-range collisions in the LHC. Figure 4 shows the SPS beam lifetime at 26 GeV/c measured as a function of the beam-wire separation d under these conditions. The observed dependence is perfectly fitted by a 5th order power law of the form

$$\tau \approx 5 \text{ms} \left(\frac{d}{\sigma} \right)^5. \quad (5)$$

A naive extrapolation to the typical LHC separation of 9.5σ yields a beam lifetime of about 6 minutes. This estimate may be too pessimistic, as tune ripple, intrabeam scattering, and other noise sources will likely be much smaller in the LHC than in the SPS. To test the assumed scaling with beam energy, it would be desirable to repeat this experiment at a proton momentum higher than 26 GeV/c.

In a second class of experiments, one SPS wire was used to compensate the effect of the other one. The betatron phase advance between the two SPS wires is about 2.6° , which equals the expected average phase advance between compensator and long-range collision points in the LHC, and according to simulations is sufficiently small for the compensation to be effective [19].

Figure 5 displays the tune scan performed in one of these experiments, and Fig. 6 shows the beam lifetimes measured

Table 2: Parameters for the nominal and ultimate LHC compared with those for two alternative upgrade scenarios with either shorter bunches at 10 or 15-ns spacing [more shorter bunches], or longer more intense uniform bunches at 75-ns spacing [large Piwinski angle].

parameter	symbol	nominal	ultimate	shorter bunches	longer bunches
no. bunches	n_b	2808	2808	4680	7020
protons/bunch	$N_b [10^{11}]$	1.15	1.7	1.7	6.0
bunch spacing	$\Delta t_{\text{sep}} [\text{ns}]$	25	25	15	10
average current	$I [\text{A}]$	0.58	0.86	1.43	2.15
norm. transv. emittance	3.75	3.75	3.75	3.75	3.75
longit. profile		Gaussian	Gaussian	Gaussian	uniform
rms bunch length	$\sigma_z [\text{cm}]$	7.55	7.55	3.78	20
beta function at IP1&5	$\beta^* [\text{m}]$	0.55	0.5	0.25	0.25
crossing angle	$\theta_c [\mu\text{rad}]$	285	315	445	430
Piwinski angle	$\Theta \equiv \theta_c \sigma_z / (2\sigma^*)$	0.64	0.75	0.75	2.8
luminosity	$L [10^{34} \text{ cm}^{-2} \text{ s}^{-1}]$	1.0	2.3	7.7	11.5
events/crossing		19	44	88	510
rms length of luminous region	$\sigma_{\text{lum}} [\text{mm}]$	44.9	42.8	21.8	36.3

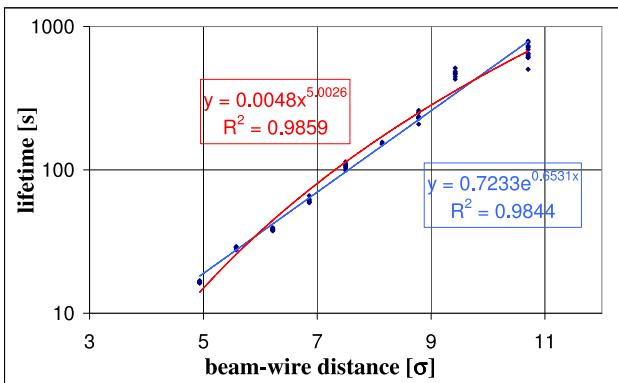


Figure 4: SPS beam lifetime measured as a function of the beam-wire distance, in an experiment conducted on 09/11/2004, with a single-wire excitation of 190 A, tunes $Q_x = 0.3208$, $Q_y = 0.2914$, emittance $\gamma\epsilon_x \approx \gamma\epsilon_y \approx 1.4 \mu\text{m}$, and an rms beam size of about 1.56 mm. The beam was separated from the wire in the vertical direction.

at these tunes without any wire, with a single wire, and with a two-wire compensation. The beam lifetime, which drops for a single wire, is recovered by the second wire over a large range of tunes, except for at $Q_y < 0.285$. The reason why the compensation failed for lower tune values is not understood. Repeating this experiment would be worthwhile, in order to verify that this apparent lack of compensation was not an artifact of changing beam conditions in the injectors.

2.2 Simulations

A new simulation code, called BBTRACK, was written in 2005 [20], for the purpose of weak-strong simula-

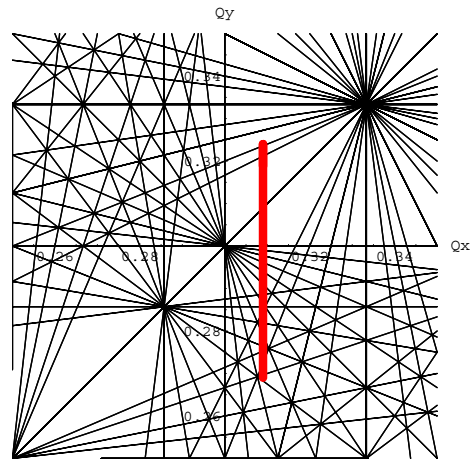


Figure 5: Tune path traced during the first SPS wire-compensation experiment on 30/07/04., and resonance lines through 11th order.

tions of long-range and head-on beam-beam interactions and wire compensation. The programming language is FORTRAN90. The model implemented in BBTRACK is similar to those of WSDIFF [2, 21] and Irwin [18]. In addition to BBTRACK and WSDIFF, yet another code used for LHC long-range beam-beam studies is BBSIM, developed at FNAL [22].

Figure 7 illustrates the effect of the second compensating wire on the stable region in the $x - y$ plane, as simulated by BBTRACK. The irregular shape of the stability boundary, observed for a single wire, relates to resonance islands. The boundary becomes a smooth rectangle when the second wire is active.

Figure 8 shows that the second wire increases the dy-

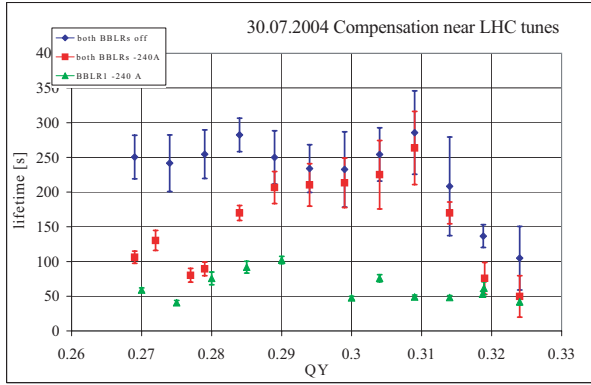


Figure 6: Beam lifetimes measured as a function of the vertical tune without BBLR (blue diamonds), with one BBLR excited at 240 A (green triangles) and with both BBLRs excited so that they compensate each other (red squares), on 30/07/04.

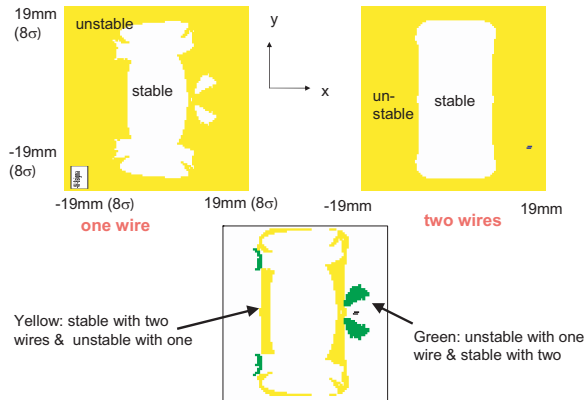


Figure 7: Simulated stability region in the x - y plane for the SPS with one (top left) and two wires (top right), and the difference (bottom). The horizontal and vertical scales both extend over $\pm 8\sigma$. The wire current is 240 A and the horizontal beam-wire distance 19 mm. The simulation was performed with BBTRACK.

dynamic aperture by about 1σ from 3σ to 4σ , independent of the betatron phase, for the SPS parameters considered.

A closer look at unstable trajectories reveals that the chaotic particles jump between quasi-regular phase-space ellipses when they approach the wire (or, in the LHC, the other beam). An example of an unstable trajectory in the horizontal phase space is shown in Fig. 9.

The sensitivity to the transverse position of the second wire was both measured and simulated. Figure 10 compares the SPS experiment and a simulation with the BBSIM code [23]. Either one shows that the transverse position has to be controlled to within 2–3 mm (or 10%-15% of the total distance), in order to observe a positive effect of the compensating wire. A similar tolerance is also found by the BBTRACK code, in Fig. 11.

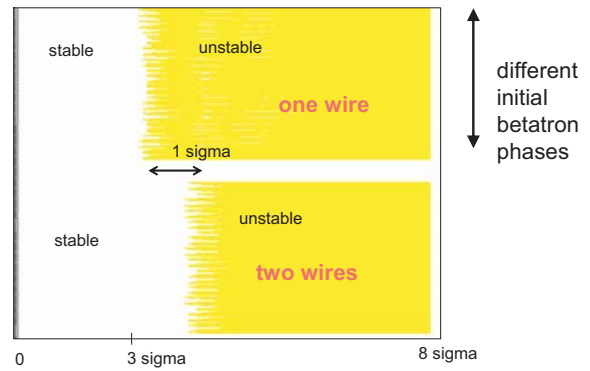


Figure 8: Simulated stability boundary (color) for the SPS as a function of horizontal starting amplitude (horizontal axis) for one (top) and two wires (bottom). The different rows refer to different initial betatron phases. The wire current is 240 A and the horizontal beam-wire distance 19 mm. The simulation was performed with BBTRACK.

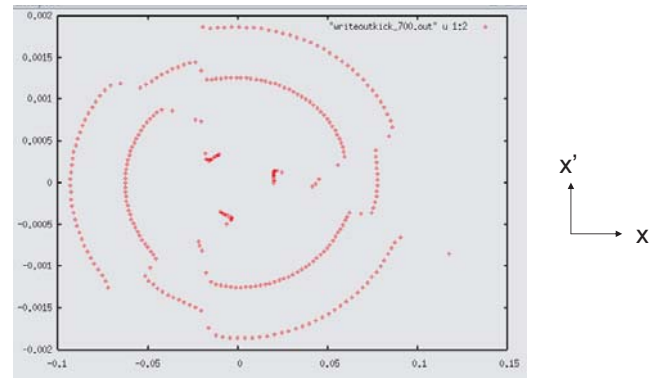


Figure 9: Unstable trajectory in the SPS from a BBTRACK simulation. Jumps between quasi-regular ellipses occur when the tracked particle comes close to the wire.

2.3 LHC Situation

Long-range beam-beam compensation for the LHC based on current-carrying wires was proposed by Koutchouk [10, 11]. Figures 12 and 13 show the schematic layout. The compensators are placed upstream of the separation dipole D1 (41 m downstream of D2), where the beams pass through two independent vacuum chambers, at a point with about equal horizontal and vertical beta function. The local correction provided by this scheme compensates all nonlinear effects.

Figure 14 illustrates the reduction of the LHC tune spread from long-range collisions by such a compensator.

In view of the promising predictions and SPS experimental results, for future LHC wire compensators — “BBLRs” — 3-m long sections have been reserved in the LHC at a distance of 104.93 m (center position) from the main collision points on either side of IP1 and IP5 (see

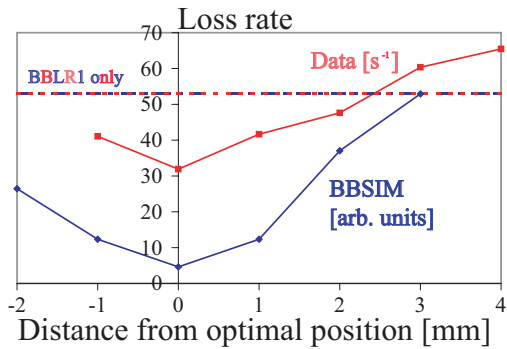


Figure 10: Relative SPS beam loss rate in s^{-1} , as measured over 2.4 s, and simulated loss rate in arbitrary units vs. the vertical position of the compensating second wire. Measured and simulated loss rates for a single wire are indicated by the two superimposed straight lines.

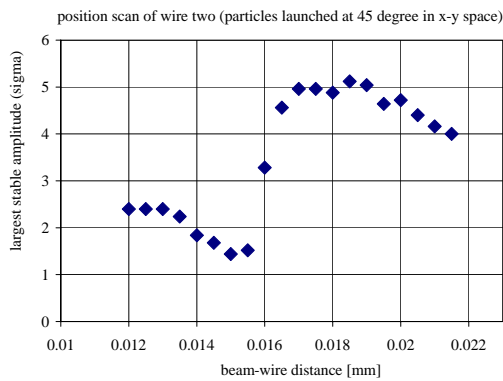


Figure 11: Maximum stable amplitude (dynamic aperture) as a function of the vertical position of the second wire simulated by the code BBTRACK. The distance of the first wire is held constant at 19 mm.

Fig. 15) [24].

Figure 16 shows the tune footprint generated by long-range collisions in LHC IP1 and IP5 for a nominal bunch and an extreme PACMAN bunch. The tune spread of the PACMAN bunch is half that of the nominal one, because the former experiences half the number of long-range collisions.

Figure 17 shows the reduction in the tune footprint for a nominal bunch achieved by the nominal wire compensation. Because in the final triplets the bunches are no longer round, and there also is a small average phase advance (2.6°) between compensator and long-range collisions, the compensation is not perfect.

An equivalent footprint for an extreme PACMAN bunch is displayed in Fig. 18. For this PACMAN bunch the compensation is twice too strong, as half of the long-range collisions are absent and the wire overcompensates. This overcompensation leads to a ‘flip’ of the tune footprint.

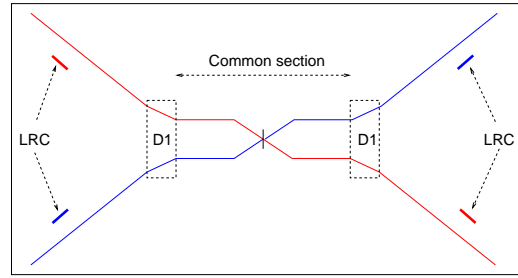


Figure 12: Schematic position of the long-range correctors at IP1 or IP5 of LHC [11].

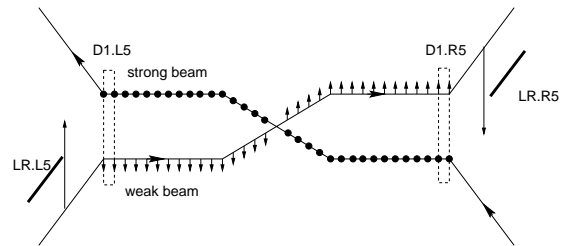


Figure 13: Positions of the proposed long-range correctors and of all long-range collisions around one IP in LHC [10].

Figures 19 and 20 shows the same set of tune footprints, namely with and without wire compensation for a nominal and an extreme PACMAN bunch, respectively, only that in this case the head-on collision is also included. In Fig. 19 the tune spread of a nominal bunch is much reduced. Most of the long-range effect is removed. In Fig. 20, the tune shift of the PACMAN bunch changes its appearance. The tune footprint with compensation becomes narrower and

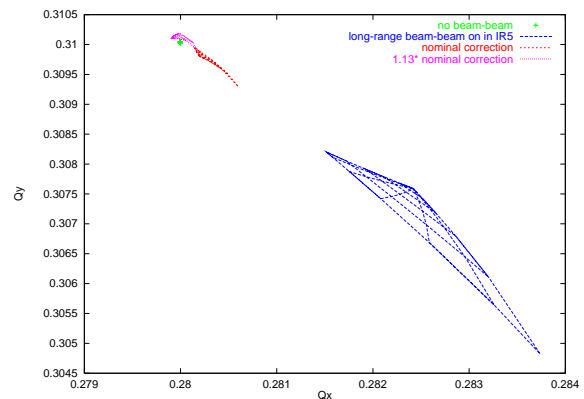


Figure 14: Tune footprint due to long-range collisions in IR5, without wire compensation, with a nominal wire and with an empirically adjusted wire current equal to 1.15 times the nominal [10]. The tune footprint was calculated by MAD8 tracking for start amplitudes up to 6σ .


<p>CERN CH-1211 Geneva 23 Switzerland</p>  <p>the Large Hadron Collider project</p>			<p>LHC Project Document No. LHC-BBC-EC-0001</p> <p>EDMS Document No. 503722</p> <p>Engineering Change requested by (Name & Div./Grp.): C.Fischer AB/BDI</p>
<p>Date: 2004-10-27</p>			
<p>Engineering Change Order – Class I</p> <p>RESERVATIONS FOR BEAM-BEAM COMPENSATORS IN IR1 AND IR5</p> <p><i>Brief description of the proposed change(s):</i></p> <p>Reservations on the vacuum chamber in IR1 and IR5 for beam-beam compensator monitors. We propose to include these modifications in the next v.6.5 machine layout version.</p>			
<p>Equipment concerned : BBC</p>	<p>Drawings concerned : LHCLX-0001 LHCLX-0002 LHCLX-0009 LHCLX-0010</p>	<p>Documents concerned :</p>	
<p>PE in charge of the item : J.P. Koutchouk AT/MAS</p>	<p>PE in charge of parent item in PBS : C. Rathjen AT/VAC</p>		
<p>Decision of the Project Engineer :</p> <ul style="list-style-type: none"> Rejected. Accepted by Project Engineer, no impact on other items. <i>Actions identified by Project Engineer</i> <p>Z Accepted by Project Engineer, but impact on other items. <i>Comments from other Project Engineers required</i> <i>Final decision & actions by Project Management</i></p>	<p>Decision of the PLO for Class I changes :</p> <ul style="list-style-type: none"> Not requested. Rejected. <p>Z Accepted by the Project Leader Office. <i>Actions identified by Project Leader Office</i></p>		
<p>Date of Approval : 2004-10-27</p>	<p>Date of Approval : 2004-10-27</p>		
<p>Actions to be undertaken : Modify the drawings and Equipment codes concerned to reflect the changes described in this ECO.</p>			
<p>Date of Completion : 2004-10-27</p>	<p>Visa of QA Officer :</p>		
<p><small>Note : when approved, an Engineering Change Request becomes an Engineering Change Order/Notification.</small></p>			

Figure 15: Cover page of LHC engineering change order, reserving space for beam-beam compensators at 104.93 m from IP1 and IP5 [24].

more elongated. At the same time, it seems to be ‘twisted’, which likely is bad for stability.

Figure 21 presents the result of a vertical tune scan for a nominal LHC bunch. Shown are the stable and unstable regions (color code) as a function of starting amplitude along the 45-degree direction, $x = y$, (vertical axis) and as a function of tune (horizontal axis). The amplitude scale extends from 0 to 10σ . The upper graph refers to long-range and head-on collisions without compensation. The bottom graph also includes the compensation. The figure demonstrates that particles are stabilized through 10σ in several wide tune regions.

Figure 22 present an analogous result for a PACMAN bunch. The PACMAN bunch is much more stable without wire compensation, since it suffers only a smaller number of long-range collisions. However, the wire compensation acts strongly destabilizing for almost all tunes. Comparing Figs. 21 (top) and 22 (bottom) we infer that the extreme PACMAN bunch with compensation is (at least) as unstable as the nominal bunch without compensation.

Figure 23 and 24 present the results of Figs. 21 and 22 in a slightly different way (better suited for black & white printers). Shown is the dynamic aperture, defined by the amplitude of the first unstable trajectory, as a function of

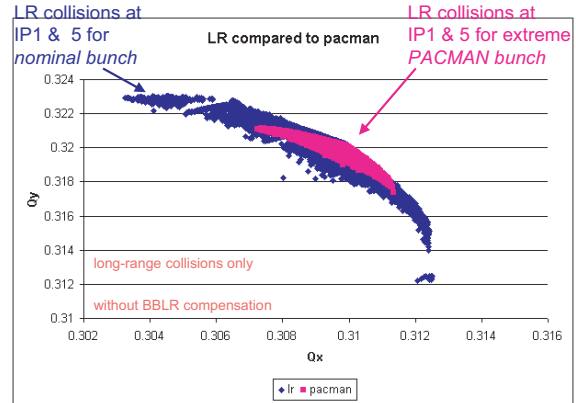


Figure 16: LHC tune footprint with only long-range collisions at IP1 and IP5 for a nominal and an extreme PACMAN bunch, computed by BBTRACK.

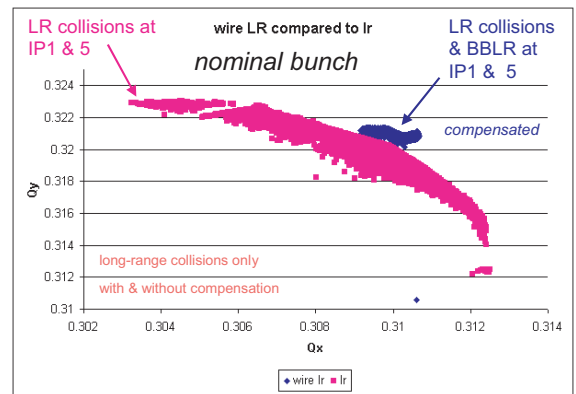


Figure 17: LHC tune footprint with only long-range collisions at IP1 and IP5 with and without wire compensation for a nominal bunch, computed by BBTRACK.

the vertical tune. The blue and red curves refer to the situations without and with wire compensation. Figure 23 representing a nominal bunch shows that the wire increases the dynamic aperture by about 2σ . Figure 24 reiterates that for an extreme PACMAN bunch about the same amount of dynamic aperture is lost due to overcompensation. In all these simulations we assume that a dc wire compensator is employed. The reduction in dynamic aperture would of course not occur in case of a pulsed wire with decreasing strength for the PACMAN bunches.

The long-range collisions and their compensation can also lead to 6-dimensional effects, e.g., to an additional chromaticity, which would be different for the nominal and the PACMAN bunches. Figure 25 displays the dispersion and beta functions in the two main interaction regions. The peak vertical dispersion generated by the vertical crossing angles, and to a lesser extent by the detector fields of LHCb and ALICE, reaches a value of 1 m inside the final triplet.

The chromaticity induced by the long-range beam-beam

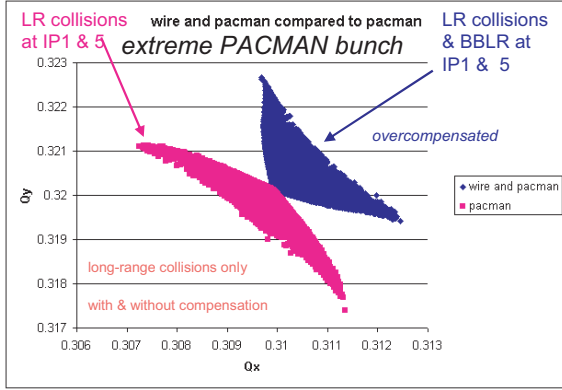


Figure 18: LHC tune footprint with only long-range collisions at IP1 and IP5 with and without wire compensation for an extreme PACMAN bunch, computed by BBTRACK.

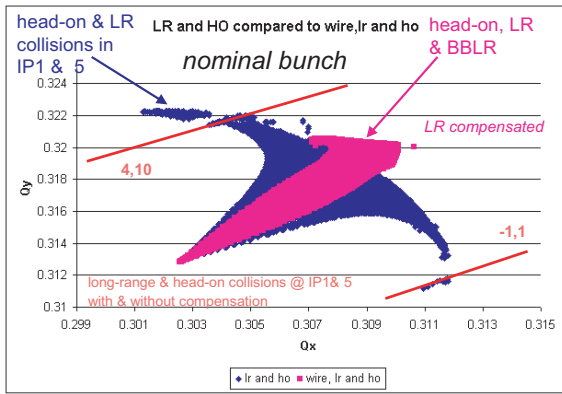


Figure 19: LHC tune footprint with long-range and head-on collisions at IP1 and IP5 with and without wire compensation for a nominal bunch, computed by BBTRACK.

collisions (or by a wire) was calculated by Erdelyi and Sen [25]:

$$\begin{aligned}
 Q' &= \left(\frac{r_p N_b}{4\pi\epsilon_N} \right) \frac{4}{d^6} (d_x^3 \eta_x + 3d_x^2 d_y \eta_y \\
 &\quad - 3d_x d_y^2 \eta_x - d_y^3 \eta_y) n_{LR} \\
 &\approx \left(\frac{r_p N_b}{4\pi\epsilon_N} \right) \frac{4}{d_{x,y}^3} \frac{D_{x,y}}{\sqrt{\beta\epsilon}} n_{LR}, \quad (6)
 \end{aligned}$$

where $d = \sqrt{d_x^2 + d_y^2}$ denotes the transverse distance between the beams (or between beam and wire), normalized to the rms beam size σ (round beams are considered), n_{LR} is the number of long-range collisions, $\eta_{x,y}$ the dispersion function $D_{x,y}$ also normalized to σ , ϵ_N the normalized emittance and ϵ the geometric one.

Inserting typical values (Fig. 25) of $D \approx 0.6$ m, $\beta \approx 3$ km, $n_{LR} = 30$ and $d = 9.5$, we obtain $Q' \approx 0.25$, which is a small effect, albeit perhaps measurable.

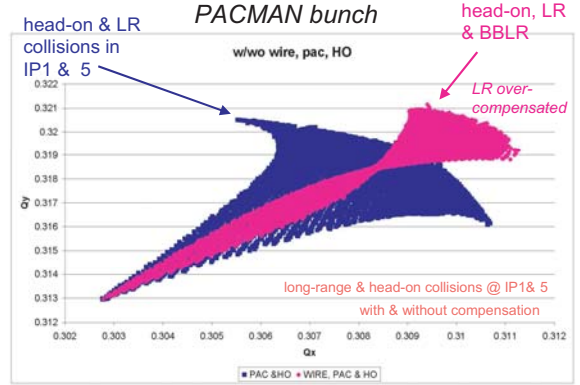


Figure 20: LHC tune footprint with long-range and head-on collisions at IP1 and IP5 with and without wire compensation for an extreme PACMAN bunch, computed by BBTRACK.

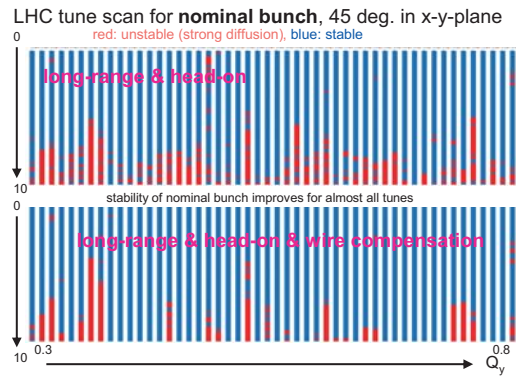


Figure 21: LHC tune scan for a nominal bunch. Shown are stable (blue) and unstable (red) start amplitudes in descending order without (top) and with wire compensation (bottom) as a function of the vertical tune, for a constant horizontal tune of $Q_x = 0.31$, computed by BBTRACK.

2.4 RHIC Experiment

Experimental demonstration of long-range compensation at an operating hadron collider would be extremely valuable before embarking on an installation at the LHC. The RHIC collider offers almost ideal conditions, except that the number of long-range collisions which could be compensated is limited to about 1, to be compared with 30 per IP in LHC. Initial simulations predicted a marginal effect of a single long-range collision in RHIC.

A RHIC machine experiment was conducted at injection energy on April 28, 2005, with a single bunch per ring. The two beams (called ‘yellow’ and ‘blue’) were brought into long-range collision either at a main IP (IP4) or shifted by about 10.65 m longitudinally, namely to the position for which an effective compensator could be installed. The experiment measured the lifetime of both beams as a function of the transverse separation. The latter was varied between

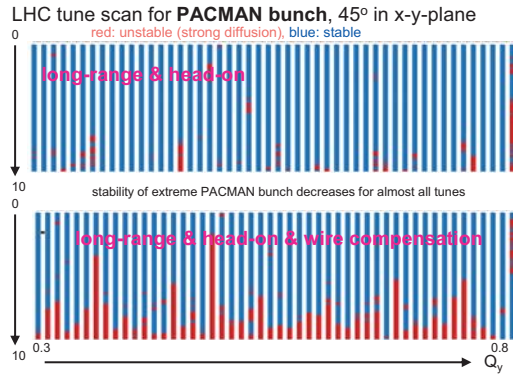


Figure 22: LHC tune scan for an extreme PACMAN bunch. Shown are stable (blue) and unstable (red) start amplitudes in descending order without (top) and with wire compensation (bottom) as a function of the vertical tune, for a constant horizontal tune of $Q_x = 0.31$, computed by BBTRACK.

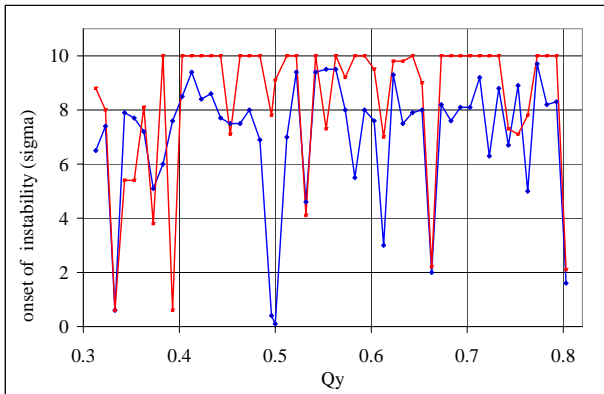


Figure 23: LHC tune scan for a nominal bunch. Shown is the dynamic aperture without (blue) and with wire compensation (red) as a function of the vertical tune, for a constant horizontal tune of $Q_x = 0.31$, computed by BBTRACK.

11 and 2σ . Various example scans (courtesy W. Fischer) are shown in Figs. 26–29. The experiment demonstrated a measurable effect and it revealed that the beam loss is very sensitive to the working point, which may explain the great differences in the response of the two beams. Parameters other than the orbit were changed (not shown in the plot). The last scan, in Fig. 29, is thought to be the most relevant one.

Figure 30 presents results from a recent simulation with BBTRACK for the RHIC experiment. The simulation predicts an increased particle loss for beam-beam separations of less than 6σ . The simulated threshold at 6σ appears consistent with many of the experimental results in Figs. 26–29. Figure 31 shows that the simulated effect is quite sensitive to the precise tune value, a feature which was also noticed in the experiment.

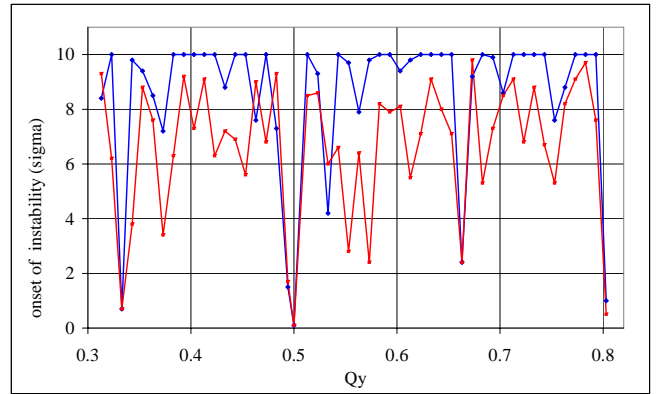


Figure 24: LHC tune scan for an extreme PACMAN bunch. Shown is the dynamic aperture without (blue) and with dc wire compensation (red) as a function of the vertical tune, for a constant horizontal tune of $Q_x = 0.31$, computed by BBTRACK.

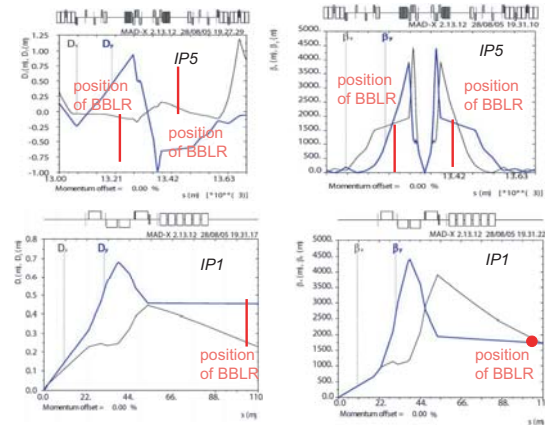


Figure 25: The LHC design dispersion (left) and beta functions (right) on either side of IP5 (top) and on the right side of IP1 (bottom). The foreseen position of the wire compensators is indicated by the vertical red lines or dot, respectively.

2.5 US LARP

The wire compensation at RHIC and related studies have become part of the US LHC Accelerator Research Program under the task name “wire compensation of beam-beam interactions” [26]. The persons responsible for this task are Wolfram Fischer and Tanaji Sen. The CERN contacts are Jean-Pierre Koutchouk and Frank Zimmermann. The work proposed by this US LARP task force for the US fiscal year 06 includes the design and construction of a wire compensator either at BNL or FNAL, the installation of this wire compensator on a movable stand in one of the two RHIC rings, theoretical studies (analysis and simulations) to test the compensation and its robustness, beam studies in RHIC with 1 bunch per beam at flat top and 1 parasitic interaction,

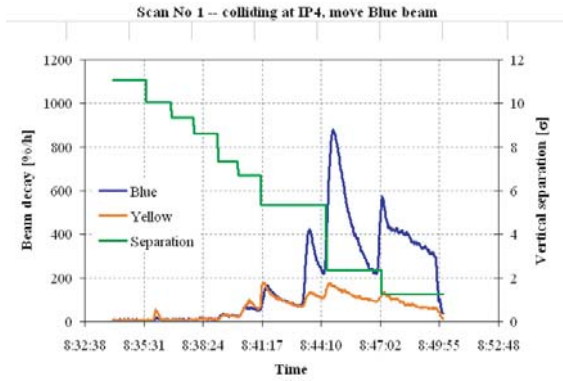


Figure 26: RHC experiment on 28 April 2005, scan no. 1, two bunches collide at IP4; the blue beam is moved vertically; the lifetimes of both beams and their separation are shown as a function of time.

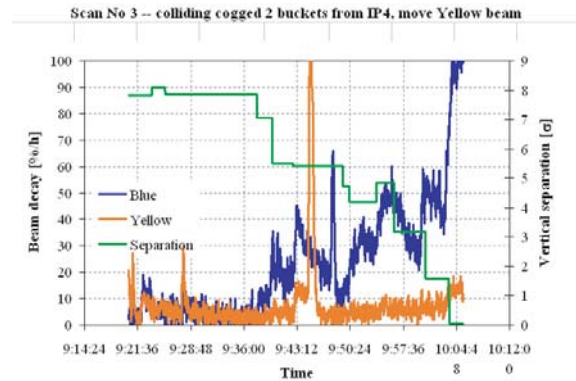


Figure 28: RHC experiment on 28 April 2005, scan no. 3, two bunches collide 10.65 m from IP4; the yellow beam is moved vertically; the lifetime of both beams and their separation is shown as a function of time.

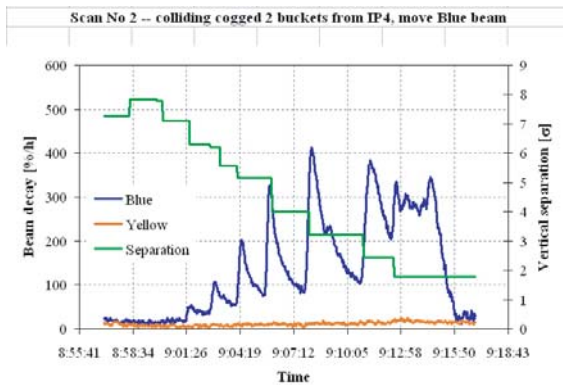


Figure 27: RHC experiment on 28 April 2005, scan no. 2, two bunches collide 10.65 m from IP4; the blue beam is moved vertically; the lifetime of both beams and their separation is shown as a function of time.

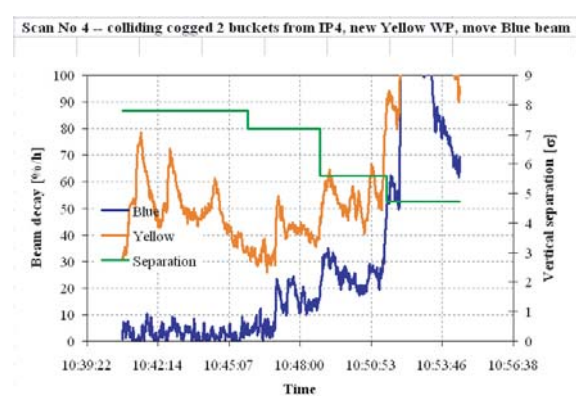


Figure 29: RHC experiment on 28 April 2005, scan no. 4, two bunches collide 10.65 m from IP4; a new working point was chosen for the yellow beam; the blue beam is moved vertically; the lifetime of both beams and their separation is shown as a function of time.

observations of lifetimes, losses, emittances, tunes, orbits for each beam-beam separation, as well as beam studies to test tolerances on the beam-wire separation with respect to the beam-beam separation, on the wire current accuracy, and on the current ripple. For fiscal year 07, it is planned to conduct beam studies with elliptical beams at the parasitic interaction point, choosing an aspect ratio close to that of the beam in the LHC IR quadrupoles, and to compensate multiple bunches in RHC with a pulsed wire current, requiring an additional voltage modulator.

2.6 Pulsed Wire

The above simulation results for the LHC (Figs. 21–24) show that while the compensator improves the dynamic aperture of the nominal bunches it reduces the one of the extreme PACMAN bunches. In order to avoid a possible lifetime degradation for the PACMAN bunches the compensator should be pulsed train by train.

Figure 32 shows the nominal LHC filling pattern, with

gaps of various lengths between trains reflecting the rise times of kickers needed for the beam transfers between different injectors and also between the SPS and the LHC. The wire current needs to be ramped up at the start of each bunch train and ramped down to either zero or an intermediate value (depending on the length of the gap) at the end of each train. Zooms of the required excitation patterns over the first few trains are displayed in Fig. 33. The total number of 72-bunch trains stored in the LHC is 39. Therefore, the wire would need to be pulsed 39 times per revolution period or at about 440 kHz. This pulsing rate is considered challenging and it is believed to exclude IGBT technology for the pulser [27], which instead should be based on MOSFETs.

The requirements for pulsed wire are summarized in Table 3, both for the LHC and for a hypothetical SPS prototype. The main challenges appear to be the high repetition rate and the turn-to-turn stability tolerance.

Table 3: Specifications for LHC pulsed-wire compensator and possible SPS prototype.

	LHC	SPS
revolution period T_{rev} (pattern repetition frequency)	$88.9 \mu\text{s} \pm 0.0002 \mu\text{s}$ (variation with beam energy)	$23.5 \mu\text{s} \pm 0.02 \mu\text{s}$ (variation with beam energy)
maximum strength	120 Am	120 (or 72) Am
maximum current	120 A (1 m) or 60 A (2 m)	100 (60) A
total ramp up/down time from/to zero	374.25 ns	374.50 ns
length pf maximum excitation	1422.15 ns	1423.12 ns
lengths of minimum excitation (larger minimum times may be needed too)	573.85 ns & 598.8 ns	574.24 ns & 599.21 ns
length of abort gap (could vary)	2594.75 ns	1398.17 ns
number of pulses per cycle	39	3 (4) or 10
average pulse rate	439 kHz	130 (173) or 433 kHz
pulse accuracy with respect to ideal	5%	5%
turn-to-turn amplitude stability (rel.)	10^{-4}	10^{-4}
turn-to-turn timing stability	0.04 ns	0.04 ns

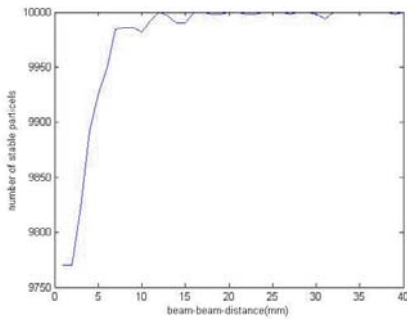


Figure 30: BBTRACK simulation of the RHIC experiment on 28 April 2005. Shown is the number of particles surviving over 300000 turns as a function of the beam-beam distance. Initially 10000 particles were distributed on a grid extending from -8σ to $+8\sigma$ in x and y . The unperturbed tunes are $Q_x = 0.27$ and $Q_y = 0.28$.

Approaches towards a pulsed-wire solution are manifold:

- An earlier design exists for a pulsed LHC orbit correction by G. Lambertson and J. Corlett [28, 29]. This system was expensive ten years ago.
- Fast kicker developments for the ILC are ongoing at KEK [30] and other laboratories.
- Fast switching devices have been developed for induction rf systems [31].
- Contacts with European industry have been established.
- A collaboration with US LARP has been set up, which includes the pulsed wire option.
- Advice by Fritz Caspers and other CERN colleagues provides input.

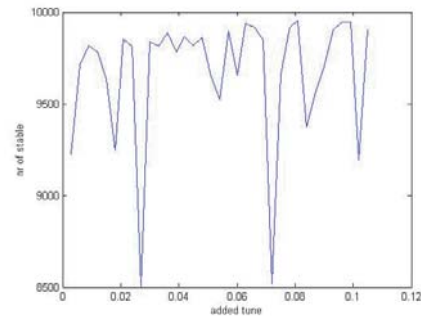


Figure 31: BBTRACK simulation of the RHIC experiment on 28 April 2005. Shown is the number of particles surviving over 300000 turns as a function of a shift in the vertical tune for a constant beam-beam distance of 3σ . Initially 10000 particles were distributed on a grid extending from -8σ to $+8\sigma$ in x and y . The unperturbed tunes, computed from the RHIC model optics without beam-beam interaction and without the additional shift, are $Q_x = 0.27$ and $Q_y = 0.28$.

- A paper study by U. Dorda is underway.
- If a promising solution is found, a lab test set up at CERN can be considered.
- The US LARP aims for an experimental test of a pulsed wire at RHIC in 2007.

2.7 Summary of Wire Compensation

Long-range compensation was demonstrated in the CERN SPS using 2 wires. The main indicator is the recovery of the unperturbed beam lifetime. Computer simulations predict 1–2 σ gain in dynamic aperture for the nominal LHC. The wire compensator would allow keeping the same – or even a lower – crossing angle for higher beam

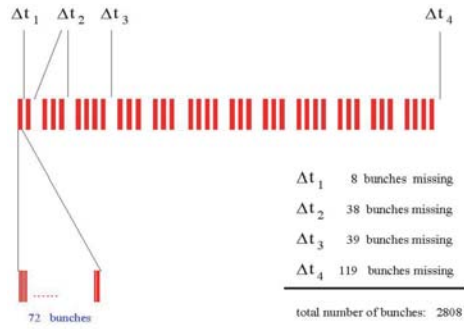


Figure 32: The nominal LHC filling pattern [1].

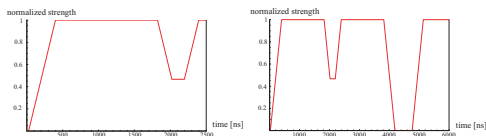


Figure 33: Examples of pulsed-wire excitation patterns for LHC (zoom).

current, thereby greatly reducing the geometric luminosity loss.

2.8 Wire Challenges and Plans

Further SPS experiments are foreseen. A 3rd wire device, already constructed, will be installed in 2007. RHIC experiments will demonstrate the effectiveness of wire compensation with real colliding beams. Options for a pulsed wire are under study. The main challenges are the required tight jitter tolerance and the high repetition rate of the pulser.

3 CRAB CAVITIES

3.1 History and Status

Crab cavities were first proposed for linear colliders by R. Palmer in 1988 [12]. Soon the concept was extended to storage-ring colliders by K. Oide and K. Yokoya [13]. The crab-cavity scheme is illustrated in Fig. 34, for the proposed Super-KEKB collider. There are two crab cavities per beam and per IP. Before the IP, the first crab cavity introduces a transverse deflection of opposite sign for the head and tail of the bunch, in such a way that the collision becomes to first order equivalent to a head-on collision, without any geometric luminosity reduction. The second cavity, on the outgoing side cancels the effect of the first cavity, on the other side of the IP.

The first installation of crab cavities in an operating collider is foreseen for the end of 2005 at the present KEK B factory [35], with only one cavity per ring and different closed orbit for particles in the head and tail of a bunch.

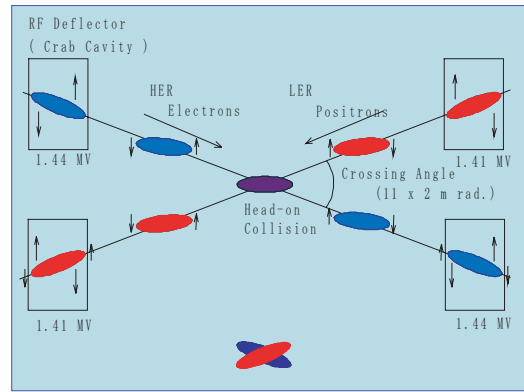


Figure 34: Schematic of crab crossing at SuperKEKB [32].

Figures 35–37 illustrate some of the fabrication and processing steps for the KEKB superconducting crab cavities. The main motivation for the KEKB and Super-KEKB crab cavities is the prediction by simulations that they will increase the beam-beam tune shift by a factor of two or more [4].



Figure 35: Barrel polishing of KEKB crab cavity [33].



Figure 36: Annealing at 700°C for 3 hours of KEKB crab cavity [33].

History of s.c. crab-cavity developments is sketched as follows [34]: In the 1970's a collaboration of CERN and



Figure 37: High-pressure water rinsing by 80-bar ultra-pure water of KEKB crab cavity [33].

KfZ Karlsruhe developed a s.c. deflecting cavity at 2.86 GHz for kaon separation. In 1991, Cornell designed a 1.5-GHz crab cavity, and built 1/3 scale models, for B factory application. Since 1993 KEKB has been developing a 500-MHz crab cavity with extreme polarization, optimized for 1–2 A of beam current and 5–7 mm bunch lengths. From 2000 onwards FNAL is constructing a deflecting cavities for the CKM (“charged kaons at the main injector”) experiment. In 2003, KEK made a new crab cavity design for Super-KEKB, which can sustain 10 A beam current and 3 mm bunch lengths. This cavity is more heavily damped than the previous ones. The damping is accomplished by a combination of coaxial couplers and wave guides. Recently Daresbury laboratory started studying crab cavities for the ILC. Cornell and LBNL expressed interest in developing crab cavities for the Super-LHC.

3.2 Voltage Requirement

The geometric luminosity loss for a large crossing angle can be reduced either by bunch shortening rf or by crab cavity rf. It is instructive to compare the voltage required for the two cases.

The voltage required for bunch shortening is

$$V_{\text{rf}} \approx \left[\frac{\epsilon_{||,\text{rms}}^2 c^3 C \eta}{E_0 e \pi f_{\text{rf}}} \right] \frac{1}{\sigma_z^4} \approx \left[\frac{\epsilon_{||,\text{rms}}^2 c^3 C \eta}{E_0 e \pi f_{\text{rf}}} \right] \frac{\theta_c^4}{0.7^4 16 \sigma_x^{*4}}, \quad (7)$$

where in the second step we have assumed that the Piwinski angle Θ is held constant at a value of about 0.7.

Equation (7) reveals an unfavorable scaling of the rf voltage with the 4th power of the crossing angle and the inverse 4th power of the IP beam size. The voltage can be decreased, to some extent, by reducing the longitudinal emittance (but limits come from intrabeam scattering and the injectors) and increasing the rf frequency (the voltage scales inversely with the rf frequency).

Assuming horizontal crossing, the crab cavity voltage required is

$$V_{\text{crab}} = \frac{cE_0 \tan(\theta_c/2)}{e2\pi f_{\text{rf,crab}} R_{12}} \approx \frac{cE_0}{e4\pi f_{\text{rf}} R_{12}} \theta_c. \quad (8)$$

It is linearly proportional to the crossing angle and independent of the IP beam size. The voltage scales with $1/R_{12}$ where R_{12} is the (1,2) transport matrix element from the location of the crab cavity to the IP. Like the bunch shortening voltage, the crab voltage is also inversely proportional to the crab-rf frequency.

Figure 38 presents the \tilde{R}_{12} , \tilde{R}_{11} , \tilde{R}_{34} , \tilde{R}_{44} matrix elements between the IP and possible crab-cavity locations, for the nominal LHC optics. Note that the \tilde{R}_{11} from the IP to the crab cavity is the same as R_{22} for the inverse transport matrix, namely from the crab cavity to the IP, and that the \tilde{R}_{12} element equals $-R_{12}$ for the inverse transformation. The figure shows that the R_{12} or R_{34} matrix elements upstream of the final triplet are of order 30–45 m (a larger value is preferable). The R_{22} or R_{44} elements have a magnitude of about 1.

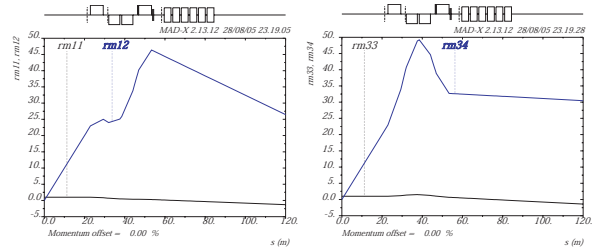


Figure 38: The horizontal matrix elements $\tilde{R}_{12} = -R_{12}$ and $\tilde{R}_{11} = R_{22}$ (left) and the vertical ones $\tilde{R}_{34} = -R_{34}$ and $\tilde{R}_{33} = R_{44}$ (right) from the IP to prospective crab-cavity locations.

The unfavorable scaling of the bunch-shortening rf voltage is illustrated in Fig. 39, where the voltage required as function of the crossing angle is compared with the corresponding crab voltage. The shortening rf voltage is typically two or three orders of magnitude higher, even if the shortening rf frequency is tripled and the longitudinal emittance reduced. Figure 40 shows zoomed view of the crab-cavity voltage as a function of crossing angle. Table 4 compiles the crab voltages required at three different crossing angles and for three different crab rf frequencies. For crossing angles up to 1 mrad, the 200-MHz system appears practical, but for larger angles it might be advantageous to increase the crab rf frequency to 400 MHz or higher, in order to reduce the total voltage.

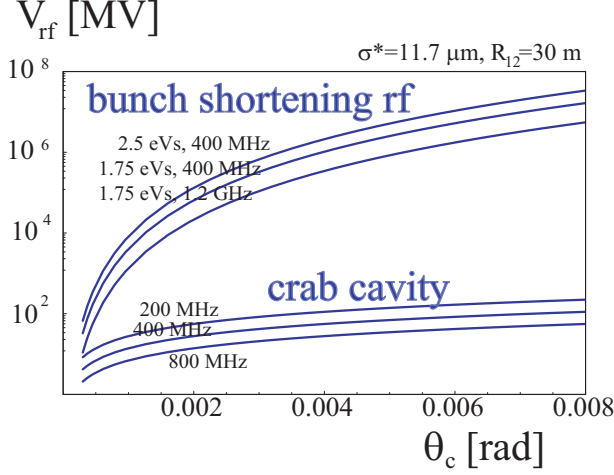


Figure 39: Bunch shortening rf voltage for $R_{\ominus} = 0.68$ and crab-cavity voltage as a function of the full crossing angle, for different rf frequencies and longitudinal emittances. The curves are computed from Eqs. (7) and (8). An IP beam size of $11.7 \mu\text{m}$ and $R_{12} = 30 \text{ m}$ from the crab cavity to the IP are assumed.

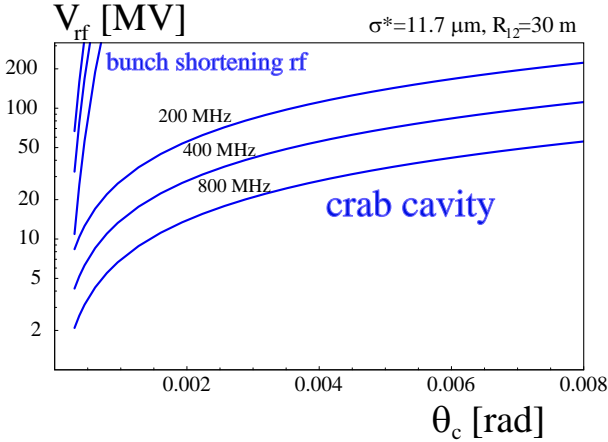


Figure 40: Zoom of Fig. 39 highlighting the crab-cavity voltage required for an LHC upgrade as a function of the full crossing angle, for different rf frequencies and longitudinal emittances. The curves are computed from Eqs. (7) and (8). An IP beam size of $11.7 \mu\text{m}$ and $R_{12} = 30 \text{ m}$ from the crab cavity to the IP are assumed.

If the R_{22} matrix element from the crab cavity to the IP is not zero, it will lead to a z -dependent additional crossing angle of the form

$$\Delta\theta_c(z) \approx \frac{R_{22}}{R_{12}} \left(\frac{\theta_c}{2} z \right). \quad (9)$$

Table 4: Super-LHC crab-cavity voltage with three different crossing angles and rf frequencies

crossing angle	0.3 mrad	1 mrad	8 mad
800 MHz	2.1 MV	7.0 MV	56 MV
400 MHz	4.2 MV	13.9 MV	111 MV
200 MHz	8.4 MV	27.9 MV	223 MV

The effect of this additional crossing angle is small, if the corresponding Piwinski angle at $z = 2\sigma_z$ is small, or if

$$\frac{(\Delta\theta_c(2\sigma_z))\sigma_z}{2\sigma_x^*} = \frac{R_{22}}{R_{12}} \frac{\theta_c \sigma_z^2}{\sigma_x^*} \ll 1, \quad (10)$$

which translates to

$$R_{22} \ll \frac{R_{12}\sigma_x^*}{\theta_c \sigma_z^2} \approx 60, \quad (11)$$

where in the last step we have assumed with $\theta_c = 1 \text{ mrad}$, $\sigma_x^{ast} = 11 \text{ m}\mu\text{m}$, $R_{12} = 30 \text{ m}$, and $\sigma_z = 7.55 \text{ cm}$. Since $|R_{22}| \approx 1$ (see Fig. 38), for a 1-mrad crossing angle this effect is insignificant.

We can do a more careful calculation of the R_{22} effect. We assume that the bunch distribution is Gaussian in the longitudinal direction and also in the plane of the crossing angle, taken to be the horizontal one,

$$\rho_x(x) = \frac{1}{\sigma_x \sqrt{2\pi}} \exp\left(-\frac{x^2}{2\sigma_x^2}\right), \quad (12)$$

$$\rho_z(z) = \frac{1}{\sigma_z \sqrt{2\pi}} \exp\left(-\frac{z^2}{2\sigma_z^2}\right). \quad (13)$$

Without crab cavities, the coordinates of the two beams, called '1' and '2', can be written as

$$\begin{aligned} x_1 &= x \cos \frac{\theta_c}{2} - s \sin \frac{\theta_c}{2}, \\ s_1 &= s \cos \frac{\theta_c}{2} + x \sin \frac{\theta_c}{2}, \\ x_2 &= x \cos \frac{\theta_c}{2} + s \sin \frac{\theta_c}{2}, \\ s_2 &= s \cos \frac{\theta_c}{2} - x \sin \frac{\theta_c}{2}. \end{aligned} \quad (14)$$

We call L_0 the luminosity without crossing angle, namely

$$L_0 = \frac{N_b^2 f_{\text{rev}} n_b}{4\pi\sigma_x\sigma_y}. \quad (15)$$

Neglecting the hourglass effect, the luminosity with a crossing angle is written as

$$L = \frac{cN_b^2 f_{\text{rev}} n_b}{\sqrt{\pi}\sigma_y} \cos^2(\theta_c/2) \int_{-\infty}^{\infty} \int_{-\infty}^{\infty} \int_{-\infty}^{\infty} \rho_x(x_1) \rho_z(s_1 - ct) \rho_x(x_2) \rho_z(s_2 + ct) dx ds dt \quad (16)$$

$$= \frac{N_b^2 f_{\text{rev}} n_b}{4\pi\sigma_x\sigma_y} \frac{1}{\sqrt{1 + \left(\frac{\sigma_z}{\sigma_x} \tan(\theta_c/2)\right)^2}}. \quad (17)$$

To model the effect of a linear (low-frequency) crab cavity, we introduce additional terms in the equations for x_1 and x_2 (note that due to symplecticity, there must also be an x' dependent change of the particle energy, but we ignore this here):

$$\begin{aligned}
 x_1 &= x \cos \frac{\theta_c}{2} - s \sin \frac{\theta_c}{2} \\
 &\quad + s \sin \frac{\theta_c}{2} + \frac{R_{22}}{R_{12}} s (s_1 - ct) \sin \frac{\theta_c}{2}, \\
 s_1 &= s \cos \frac{\theta_c}{2} + x \sin \frac{\theta_c}{2}, \\
 x_2 &= x \cos \frac{\theta_c}{2} + s \sin \frac{\theta_c}{2} \\
 &\quad - s \sin \frac{\theta_c}{2} - \frac{R_{22}}{R_{12}} s (s_1 + ct) \sin \frac{\theta_c}{2}, \\
 s_2 &= s \cos \frac{\theta_c}{2} - x \sin \frac{\theta_c}{2}. \tag{18}
 \end{aligned}$$

The luminosity reduction factor $R \equiv L/L_0$ with respect to the ideal head-on collision can be calculated from (16), with the result

$$\begin{aligned}
 R &= \frac{|R_{12}| \sigma_x \cot(\theta_c/2) \exp\left(\frac{R_{12}^2 \sigma_x^2 \cot^2(\theta_c/2)}{8\sigma_z^4 R_{22}^2}\right)}{2R_{22} \sigma_z^2 \sqrt{\pi}} \\
 &\quad K_{1/4} \left(\frac{R_{21}^2 \sigma_x^2 \cot^2(\theta_c/2)}{8R_{22}^2 \sigma_z^4} \right). \tag{19}
 \end{aligned}$$

Figure 41 illustrates the loss in luminosity compared with a head-on collision as a function of the R_{22} value, for three different crossing angles. The parameters assumed are $\sigma_x = 11.8 \mu\text{m}$, $\sigma_z = 0.0755 \text{ m}$, and $R_{12} = 30 \text{ m}$. As a reference the geometric luminosity loss factor due to the uncompensated crossing angle would be 0.72 for a crossing angle of 0.3 mrad, 0.30 for 1 mrad and 0.04 for 8 mrad.

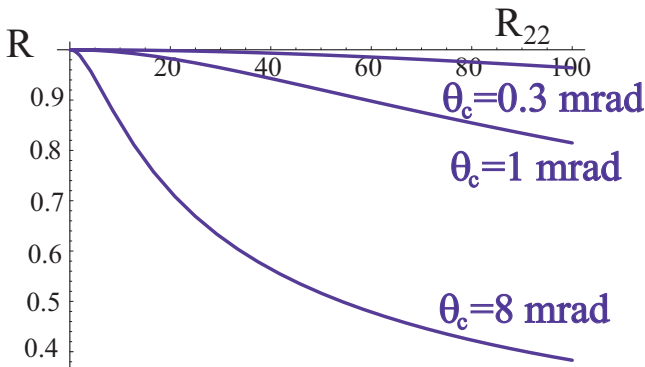


Figure 41: Residual luminosity loss factor with crab crossing as function of R_{22} for three different crossing angles, according to Eq. (19).

3.3 Space Requirement

The KEKB crab cavity provides 1.5 MV peak deflecting voltage at 500 MHz. The cavity layout is shown in Fig. 42.

It has the geometry of a squashed cell and operates in the TM2-1-0 (x-y-z) mode, which corresponds to the TM110 cylindrical mode. A coaxial coupler is used as the beam pipe. The design shown is for a standard B factory with currents of 1–2 A. For higher current, additional damping is necessary. The total length of the KEKB cell with all damping components is 1.5 m.

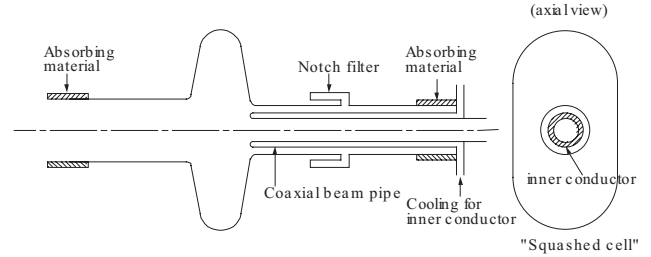


Figure 42: Schematic of squashed cell crab cavity for the KEKB factory [35, 36].

The length required for LHC can be estimated by linear scaling with the total voltage. The voltage required depends on the rf frequency. The achievable peak field may also vary with the rf frequency. Nevertheless, we can roughly estimate that 2 MV of crab voltage require a crab cavity of length 1.5 m (about the KEKB case), and 20 MV a length of 15 m. Using multi-cell instead of single-cell cavities might reduce the length compared with this simple estimate.

3.4 Crab Frequency

The crab frequency must be compatible with the bunch spacing. A frequency of 200 MHz allows for any bunch spacing which is a multiple of 5 ns. Since it has not been decided whether the upgrade will employ a bunch spacing of 10 (15) ns or 12.5 ns, a crab-cavity frequency of 400 MHz might be a safer option, with the added advantage of a factor two saving in voltage. This frequency is also close to the KEKB design.

Another constraint on the frequency is that the crab wavelength must be large compared with the bunch length. Computing the crab deflection along the bunch yields to third order in longitudinal position z (here $z = 0$ refers to the bunch center) yields

$$\Delta x'(z) \approx \frac{1}{R_{12}} \left(\frac{\theta_c}{2} z - \frac{\theta_c}{2} \frac{1}{6} \frac{c^2}{\omega_{\text{crab,rf}}^2} z^3 + \dots \right). \tag{20}$$

Demanding that the third order term is small compared with the linear term we obtain the condition

$$f_{\text{crab}} = \frac{\omega_{\text{crab,rf}}}{2\pi} \ll \frac{1}{2\pi} \frac{\sqrt{6}c}{2\sigma_z} \ll 775 \text{ MHz}, \tag{21}$$

where the nominal LHC bunch length at top energy of 7.55 cm was assumed. We conclude that 800 MHz would probably be too high.

As for the R_{22} effect, we can do a more careful calculation for the rf frequency. To model the effect of crab cavities operating at the rf wave number k_{crab} ($k_{\text{cr}} = 2\pi f_{\text{crab}}/c$), we replace in (18) the linear crab-cavity wave form by a sinusoidal one, and we take $R_{22} = 0$, since we have determined its effect earlier (we also recall here that due to symplecticity, there must also be an x' dependent change of the particle energy, which is ignored here as well):

$$\begin{aligned} x_1 &= x \cos \frac{\theta_c}{2} - s \sin \frac{\theta_c}{2} + \frac{1}{k_{\text{cr}}} \sin(k_{\text{cr}}s) \sin \frac{\theta_c}{2}, \\ s_1 &= s \cos \frac{\theta_c}{2} + x \sin \frac{\theta_c}{2}, \\ x_2 &= x \cos \frac{\theta_c}{2} + s \sin \frac{\theta_c}{2} - \frac{1}{k_{\text{cr}}} \sin(k_{\text{cr}}s) \sin \frac{\theta_c}{2}, \\ s_2 &= s \cos \frac{\theta_c}{2} - x \sin \frac{\theta_c}{2}. \end{aligned} \quad (22)$$

The luminosity reduction factor $R \equiv L/L_0$ compared with the ideal case becomes

$$R = \frac{\sqrt{1 + \cos \theta_c}}{\sqrt{2\pi}\sigma_z} \int_{-\infty}^{\infty} \exp\left(-\frac{s^2(1 + \cos \theta_c)}{2\sigma_z^2} - \frac{\sin^2(\theta_c/2)(-k_{\text{cr}}s + \sin(k_{\text{cr}}s))^2}{k_{\text{cr}}^2\sigma_x^2}\right) ds \quad (23)$$

Figure 43 illustrates the loss in luminosity compared with a head-on collision as a function of the crab frequency, for three different crossing angles. The parameters assumed are $\sigma_x = 11.8 \mu\text{m}$ and $\sigma_z = 0.0755 \text{ m}$. For comparison, the geometric luminosity loss factor due to the uncompensated crossing angle would be 0.72 for a crossing angle of 0.3 mrad, 0.30 for 1 mrad and 0.04 for 8 mrad. Crab frequencies above 400 MHz imply significant luminosity loss even for moderate crossing angles.

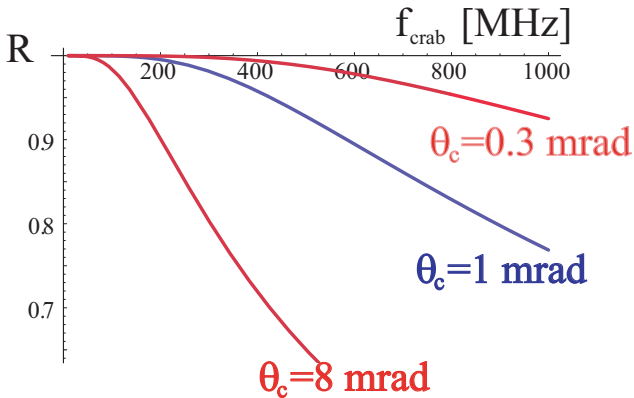


Figure 43: Residual luminosity loss factor with crab crossing as a function of crab rf frequency for three different crossing angles, according to Eq. (23).

3.5 Crab Cavity Noise

Amplitude noise introduces a small crossing angle. For example a 1% amplitude jitter would cause a crossing angle equal to 1% of the full crossing angle, which would be acceptable from the beam-beam point of view.

However, bunch slices which are longitudinally offset from the center will experience a time-varying deflection, which can lead to emittance growth. We consider a particle at position z . The noise in the crab voltage $\Delta V_{\text{crab}}/V_{\text{crab}}$ leads to the following jitter at the IP:

$$\Delta x'(z) = \frac{1}{R_{12}} \frac{\theta_c}{2} \left(\frac{\Delta V_c}{V_c} \right) z. \quad (24)$$

We assume a random noise and fast filamentation. Then, averaging over the length of the bunch, and considering two crab cavities per interaction point, the bunch emittance growth is

$$\begin{aligned} \frac{\Delta \epsilon_x}{\Delta t} &\approx n_{\text{IP}} f_{\text{rev}} \beta_x^* \left(\frac{1}{R_{12}} \frac{\theta_c}{2} \left(\frac{\Delta V_c}{V_c} \right) \right)^2 \frac{2}{\sqrt{2\pi}\sigma_z} \\ &\int_0^{\infty} z e^{-\frac{z^2}{2\sigma_z^2}} dz \\ &= n_{\text{IP}} f_{\text{rev}} \beta_x^* \left(\frac{1}{R_{12}} \frac{\theta_c}{2} \left(\frac{\Delta V_c}{V_c} \right) \right)^2 \sqrt{\frac{2}{\pi}} \sigma_z, \end{aligned} \quad (25)$$

where a factor s represents two crab cavities per IP, and n_{IP} is the number of IPs equipped with crab cavities, and f_{rev} signifies the revolution period. Inserting $R_{12} \approx 30 \text{ m}$, $n_{\text{IP}} = 2$, $\beta^* = 0.25 \text{ m}$, $\theta_c = 1 \text{ mrad}$, $\sigma_z = 7.55 \text{ cm}$, we calculate an emittance growth of 1% per hour for a relative random voltage jitter of 10^{-4} . Therefore, a 0.01% amplitude jitter is about the tolerance.

Phase noise between the cavities on the two incoming side is potentially more severe, since it causes a random offset Δx between the two beams at the main collision point. The corresponding IP deflection for small amplitude particles is

$$\Delta x' = \frac{4\pi\xi}{\beta^*} (\Delta x), \quad (26)$$

where ξ is the head-on beam-beam tune shift parameter, and the resulting emittance growth

$$\frac{\Delta \epsilon_x}{\Delta t} \approx n_{\text{IP}} f_{\text{rev}} \frac{8\pi^2 \xi^2}{\beta_x^*} (\Delta x)^2. \quad (27)$$

Inserting the same numbers as above and also $\xi \approx 0.005$, an emittance growth of 10% per hour is expected for $(\Delta x)_{\text{max}} \approx 8 \text{ nm}$.

This yields a tolerance on the left-right crab phase difference and also on the crab-main-rf phase differences. The tolerance on the left-right crab phase difference is

$$\Delta \phi \leq \frac{(\Delta x)_{\text{max}} 4\pi}{\lambda_{\text{rf}} \theta_c}. \quad (28)$$

For example, at 400 MHz this corresponds to $\Delta \phi < 0.008^\circ$ ($\Delta t < 0.05 \text{ ps}$) at $\theta_c = 1 \text{ mrad}$, or to $\Delta \phi < 0.026^\circ$ ($\Delta t < 0.18 \text{ ps}$) at $\theta_c = 0.3 \text{ mrad}$.

Table 5 compares the timing tolerance for the Super-LHC crab cavity with those of the crab cavities for KEKB, already produced, for Super-KEKB, under development, and for the ILC, under study. ILC and LHC represent an advance by about one order of magnitude in timing stability compared to the KEKB requirements. The tolerance on the relative beam-beam offset jitter is 4000 times tighter for Super-LHC than than for the ILC, but the corresponding timing jitter tolerance only 15 times. The ILC timing tolerance is believed to be within technological reach. For example, the XFEL project at DESY aims at a timing stability of 0.02 ps between different rf systems [37].

Table 5: Comparison of phase or timing tolerances for Super-LHC crab cavities with crab cavities for other projects. For KEKB and Super-KEKB, the timing tolerance corresponds to an IP offset of $0.02\sigma_x^*$, for the ILC to $0.2\sigma_x^*$, and for the LHC to one of about $5 \times 10^{-5}\sigma_x^*$.

	KEKB	Super-KEKB	ILC	Super-LHC
σ_x^*	100 μm	70 μm	0.24 μm	11 μm
θ_c	22 mrad	30 mrad	10 mrad	1 mrad
Δt	0.6 ps	0.3 ps	0.03 ps	0.002 ps

The diffusion induced by main rf phase jitter or crab cavity phase jitter for the nominal LHC was studied by K. Ohmi [35], who used the strong-strong code BBSS to infer the emittance growth as a function time for various jitter amplitudes and correlation times.

The IP position was varied as [38, 39]

$$x_N = x_{N-1} \left(1 - \frac{1}{N_c}\right) + \sqrt{\frac{2}{N_c}} (\Delta x) \xi, \quad (29)$$

where x_N is the offset at turn N , N_c the number of correlated turns and ξ a Gaussian random variable of zero mean and unit variance.

The spot size increase observed in the simulation was well fitted by a diffusion formula, where the spot size at the IP after N turns grows as

$$\sigma^2(N) = \sigma_0^2 + DN. \quad (30)$$

For a correlation time of 100 turns, Ohmi found that [35]

$$D \approx 1.4 \times 10^{-3} (\Delta x)^2, \quad (31)$$

where Δx denotes the amplitude of the (equivalent) transverse random jitter at the IP. The simulation result is illustrated in Fig. 44. From this we deduce that a 1% emittance growth over 1 hr is obtained for a 7 nm beam position jitter at the IP (corresponding to a longitudinal timing jitter of 44 μm). Ohmi expected that the tolerance for $N_c = 1$ (no correlation from turn to turn) would be 10 times tighter, i.e., 0.7 nm. This tolerance is 20 times smaller than the simple estimate of 20 nm for the LHC upgrade based on (27).

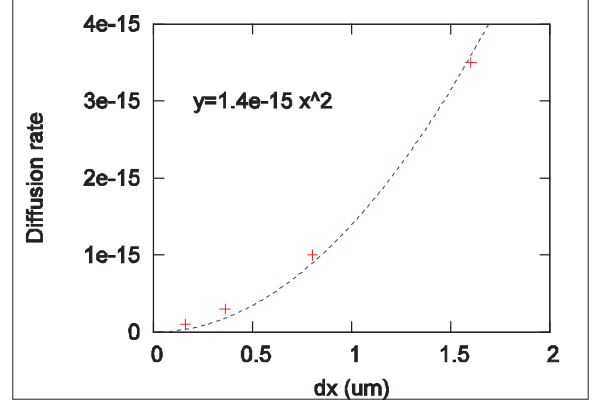


Figure 44: Diffusion rate as a function of random offset for the nominal LHC and assuming a 100-turn correlation time, as simulated by K. Ohmi [35].

Ohmi compared his simulation results with the analytical theory of Ellison, Sen and Zorzano [40, 38, 39], who derived the diffusion rate (in action) for random offset noise, in the one-dimensional case, as

$$D(a) \equiv \lim_{N \rightarrow \infty} \frac{\langle J_x^2(N) - J_x^2(1) \rangle (a)}{N} \quad (32)$$

$$= \frac{(C(\Delta x))^2}{8 - 4/N_c} \sum_{k=0}^{\infty} \frac{\sinh \theta (2k+1)^2 G_k^2(a)}{\cosh \theta - \cos[2\pi(2k+1)Q_x]},$$

where Q_x denotes the betatron tune, and

$$G_k = \frac{\sqrt{a}}{\sigma} [U'_{k+1} + U'_k] + \frac{1}{\sqrt{a}\sigma} [(k+1)U_{k+1} - kU_k], \quad (33)$$

$$U_k(a) = \int_0^a \frac{1}{w} [\delta_{0k} - (2 - \delta_{0k})(-1)^k e^{-w} I_k(w)] dw, \quad (34)$$

$$\theta = -\ln(1 - 1/N_c), \quad (35)$$

$$C = \frac{N_b r_p}{\gamma}, \quad (36)$$

$$a = \frac{\beta^* J_x}{2\sigma^2}. \quad (37)$$

The action diffusion coefficient $D(a)$ is roughly related to the beam-size diffusion coefficient D from above via

$$D \approx \frac{1}{2} \frac{\beta^2}{\sigma^2} D(a=1). \quad (38)$$

Inserting the analytical expression (32), we obtain

$$D_{\text{anal}} \approx 3 \times 10^{-5} (\Delta x)^2, \quad (39)$$

which gives a 7 times looser tolerance than the strong-strong simulation, and more in line with the estimate of (27).

In addition to the beam-beam offset, also the direct dipole kicks from random crab cavity phase jitter induce

emittance growth [41]. They may be a reason for the difference between the strong-strong simulations and the analytical estimates. The emittance resulting from dipole deflections due to random crab cavity phase jitter (regardless of beam-beam) can be estimated as

$$\frac{\Delta\epsilon}{\Delta t} \approx n_{\text{IP}} \frac{f_{\text{rev}}}{2\beta^*} \left(\frac{c\theta_c}{4\pi f_{\text{rf},\text{crab}}} \Delta\phi_{\text{crab}} \right)^2. \quad (40)$$

For example, inserting typical parameters of the LHC upgrade, $\beta^* \approx 0.25$ m, $n_{\text{IP}} = 2$, $f_{\text{rf},\text{crab}} = 400$ MHz, $4\theta_c = 1$ mrad. we find that an emittance growth of 1% per hour corresponds to a timing stability of 10 fs, a factor 3 tighter than for the ILC. This direct effect of the phase noise likely requires transverse feedback, head-tail damping, or another scheme to suppress the dipole motion.

A formula for the emittance growth including decoherence and feedback was derived by Alexahin [42], starting from the Vlasov equation. The relative emittance growth per turn is

$$\frac{1}{\epsilon} \frac{\Delta\epsilon}{\Delta t} \approx f_{\text{rev}} \frac{1-s_0}{4} \frac{(\Delta x)^2}{\sigma_x^{*2}} \frac{1}{\left(1 + \frac{g}{2\pi|\xi|}\right)^2}, \quad (41)$$

where g is a feedback gain factor (typically $g \approx 0.2$), $|\xi|$ the total beam-beam parameter (≈ 0.01), σ_x^* the horizontal IP beam size, and $s_0 \approx 0.645$ is related to the fact that only a small fraction of the energy received from a kick is imparted into the continuum eigenmode spectrum leading to an irreversible emittance growth. From formula (41), the random beam-beam offset (Δx) resulting in 1% emittance growth per hour is 1.5 nm. Without feedback ($g = 0$) the tolerance for the beam-beam random offset jitter (Δx) is 0.6 nm.

3.6 Crab Cavity Beam Dynamics

The combination of crossing angle and crab cavity is not exactly equal to the head-on collision case. Only in linear order the two situations are thought to be identical [4]. However, simulations for Super-KEKB suggest that for lepton colliders the ultimate beam-beam tune shift is the same, despite of the additional nonlinear transformations present in the case of a crab cavity [4]. For protons, without radiation damping, the differences could matter. A beam dynamics analysis is needed. Such analysis could start from the Lorentz boost of Hirata [43], taking into account the properties of the ‘synchrobeam mapping’ [44]. One question to be answered is whether the tune footprint for a crossing collision with crab cavities equals that of a head-on collision and, if not, how it differs.

3.7 Crab Cavity Impedance

The transverse impedance of a crab cavity is an issue due to the desired large beta function at the crab cavity location. For rough estimate, we may assume that the instability rise

time due to 1 crab cavity equals the rise time of about 10 normal rf cavities with the same total voltage [45].

The impedance does not need to be significant. Two designs of extremely low-impedance crab cavities have been developed for Super-KEKB. In one case coaxial couplers are used for damping the unwanted lower-frequency parasitic mode, in the other case waveguide dampers [46]. The horizontal and longitudinal impedances computed for both designs are shown in Figs. 45 and 46.

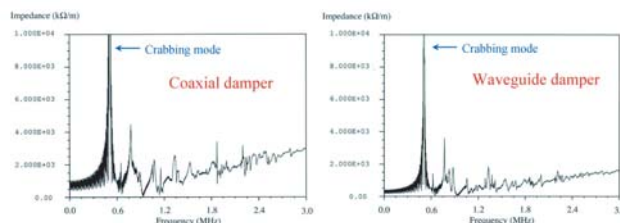


Figure 45: Horizontal impedance of two low-impedance crab cavity designs for Super-KEKB with either coaxial damping (left) or waveguide damping (right) [46].

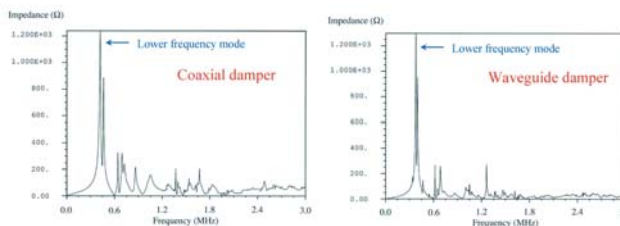


Figure 46: Longitudinal impedance of two low-impedance crab cavity designs for Super-KEKB with either coaxial damping (left) or waveguide damping (right) [46].

3.8 Summary of Crab Cavities

A first practical demonstration of crab cavities in an accelerator is expected at KEKB in early 2006. Crab cavities avoid the geometric luminosity loss, allowing for large crossing angles and, thereby, the elimination of long-range beam-beam effects. They have the additional potential of boosting the maximum beam-beam tune shift. A factor 2–3 increase in the achievable beam-beam tune shift is predicted for KEKB.

3.9 Crab Cavity Challenges and Plans

A Super-LHC crab cavity needs to be designed and prototyped. Cornell and LBNL are interested. An experimental demonstration appears necessary that the noise-induced emittance growth is acceptable for hadron colliders. The installation of a prototype and consequent experiments in RHIC would be a promising path.

4 SUMMARY

Two promising schemes — wire compensation and crab crossing — are at hand to overcome the beam-beam limitations for an LHC upgrade. Either scheme requires further experimental validation.

Individual summaries can be found in subsections 2.7 and 3.8. Plans are described in 2.8 and 3.9.

5 ACKNOWLEDGEMENTS

We thank K. Akai, G. Burtin, J. Camas, F. Caspers, W. Fischer, J.-P. Koutchouk, K. Ohmi, Y. Papaphilippou, F. Ruggiero, T. Sen, V. Shiltsev, and J. Wenninger for their important contributions to beam-beam compensation and for many helpful discussions.

6 REFERENCES

- [1] O. Bruning et al. (eds.), “LHC Design Report Vol. 1: The LHC Main Ring,” CERN-2004-003 (2004).
- [2] Y. Papaphilippou, F. Zimmermann, “Weak-Strong Beam-Beam Simulations for the Large Hadron Collider,” PRST-AB 2:104001 (1999).
- [3] H. Grote, F. Schmidt, L.H.A. Leunissen, “LHC Dynamic Aperture at Collision,” LHC Project Note 197 (1991).
- [4] K. Ohmi et al., “Luminosity Limit due to the Beam-Beam Interactions With or Without Crossing Angle,” PRST-AB 7, 104401 (2004).
- [5] W. Fischer, private communication, 29.08.2005.
- [6] V. Shiltsev, private communication, 29.08.2005.
- [7] K. Cornelis, W. Herr, M. Meddahi, “Proton Antiproton Collisions at a Finite Crossing Angle in the SPS,” PAC’91 San Francisco (1991).
- [8] J. Gareyte, “A ‘Modest’ LHC Upgrade,” Memo to F. Ruggiero and F. Zimmermann, 02.08.2001.
- [9] J. Tuckmantel, “RF and Feedback for Bunch Shortening,” Proc. CARE-HHH-APD Workshop, HHH-2004, CERN-2005-006, p. 33 (2005).
- [10] J.-P. Koutchouk, “Principle of a Correction of the Long-Range Beam-Beam Effect in LHC using Electromagnetic Lenses,” LHC Project Note 223 (2000).
- [11] J.-P. Koutchouk, “Correction of the Long-Range Beam-Beam Effect in LHC using Electro-Magnetic Lenses,” PAC 2001 Chicago (2001).
- [12] R. Palmer, “Energy Scaling, Crab Crossing, and the Pair Problem,” DPF Summer Study Snowmass ’88: High Energy Physics in the 1990’s, Snowmass, Colorado June 27–July 15 (1988).
- [13] K. Oide, K. Yokoya, “The Crab Crossing Scheme for Storage Ring Colliders,” Phys. Rev. A40: 315 (1989).
- [14] H. Hosoyama et al., “Crab Cavity for KEKB,” 7th Workshop on RF Superconductivity, Gif-sur-Yvette (1995).
- [15] F. Ruggiero, F. Zimmermann, “Luminosity Optimization Near the Beam-Beam Limit by Increasing Bunch Length or Crossing Angle,” PRST-AB 5:061001 (2002).
- [16] F. Ruggiero, F. Zimmermann, “Possible Scenarios for an LHC Upgrade,” Proc. CARE-HHH-APD Workshop, HHH-2004, CERN-2005-006, p. 1 (2005).
- [17] Y. Papaphilippou and F. Zimmermann, “Estimates of Diffusion due to Long-Range Beam-Beam Collisions,” Phys. Rev. Special Topics Accel. Beams 5:074001 (2002).
- [18] J. Irwin, “Diffusive Losses from SSC Particle Bunches due to Long-Range Beam-Beam Interactions,” SSC-233 (1989).
- [19] F. Zimmermann, “Weak-Strong Simulation Studies for the LHC Long-Range Beam-Beam Compensation,” Proc. Beam-beam workshop at Fermilab 2001, M. Xiao, T.Sen (eds), FNAL, and CERN-LHC-Project-Report-502E (2001).
- [20] Web site <http://ab-abp-bbtrack.web.cern.ch/ab-abp-bbtrack/>.
- [21] Web site <http://care-hhh-web.cern.ch/CARE-HHH/Simulation Codes/Beam-Beam/wsdiff.htm>.
- [22] Web site <http://waldo.fnal.gov/tsen/BBCODE/public>.
- [23] F. Zimmermann, J.-P. Koutchouk, F. Roncarolo, J. Wenninger, T. Sen, V. Shiltsev, Y. Paphilippou, “Experiments on LHC Long-Range Beam-Beam Compensation and Crossing Schemes at the CERN SPS in 2004,” PAC’05 Knoxville (2005)
- [24] C. Fischer, J.-P. Koutchouk, “Reservations for Beam-Beam Compensators in IR1 and IR5,” LHC Engineering Change Order, LHC-BBC-EC-0001 (2004).
- [25] B. Erdelyi, T. Sen, “Analytical Studies of the Long-Range Beam-Beam Tune Shifts and Chromaticities,” Proc. EPAC’02 Paris (2002).
- [26] T. Sen, W. Fischer, “US LHC Accelerator Research Program Task Sheet, Task Name: Wire Compensation of Beam-Beam Interactions,” 23 May 2005 (2005).
- [27] F. Caspers, private communication (2004).
- [28] J. Corlett, G. Lambertson, “Rapid Closed Orbit Correction at Interaction Points in the LHC,” LHC-Project-Note-147 (1998).
- [29] J. Corlett, “Fast Orbit Control Around Interaction Points at the Large Hadron Collider,” Talk at CERN, August 1997 (1997).
- [30] T. Naito, “ATF Kicker Studies,” Presentation at Snowmass 2005, Colorado (2005).
- [31] K. Takayama (ed.), “Proceedings of RPIA2002 — The International Workshop on Recent Progress in Induction Accelerators,” Tsukuba, Japan, 29–31 October 2002 (2002).
- [32] This picture is taken from M. Masuzawa, “Overview of Super-KEKB,” 6th Workshop on a Higher Luminosity B Factory, KEK 16–18 November 2004 (2004).
- [33] Photos are courtesy of K. Oide (2005).
- [34] The first two and the fourth development in the following list are taken from a presentation by H. Padamsee (“History of Superconducting Crab Cavity Development at Cornell and Remarks on SC Crab Cavity Development at KEK”) at the Daresbury Crab Cavity Meeting, April 2004 (2004).
- [35] K. Ohmi, “Study of Crab Cavity Option for LHC,” Proc. CARE-HHH-APD Workshop on Beam Dynamics in Future Hadron Colliders and Rapidly Cycling High-Intensity Synchrotrons “HHH-2004”, CERN-2005-006 (2005).

- [36] K. Akai et al., Proc. B factories, SLAC-400, p. 181 (1992).
- [37] E. Vogel, private communication (2005).
- [38] M.P. Zorzano, T. Sen, "Emittance Growth of the LHC Beam Due to the Effect of Head-On Beam-Beam Interaction and Ground Motion," EPAC 2000 Vienna (2000).
- [39] M.P. Zorzano, T. Sen, "Emittance Growth for the LHC Beams Due to the Effect of Head-On Beam-Beam Interaction and Ground Motion," LHC Project Note 222 (2000).
- [40] T. Sen, J.A. Ellison. "Diffusion due to Beam-Beam Interaction and Fluctuating Fields in Hadron Colliders," Phys. Rev. Lett. 77, p. 1051 (1996).
- [41] J. Tuckmantel, private communication (2005).
- [42] Y.I. Alexahin, "On the Emittance Growth due to Noise in Hadron Colliders and Methods of Its Suppression," Nucl. Instr. Meth. A 391, p. 73 (1996).
- [43] K. Hirata, "Analysis of Beam-Beam Interaction with a Large Crossing Angle," Phys. Rev. Letters 74, 12, p. 2228 (1995).
- [44] K. Hirata, H. Moshhammer, F. Ruggiero, "A Symplectic Beam-Beam Interaction with Energy Change," Part. Acc. 40, 205-228 (1993).
- [45] K. Akai, Y. Morita, "New Design of Crab Cavity for SuperKEKB," PAC 2005, Knoxville (2005).
- [46] K. Akai and Y. Morita, "New Design of Crab Cavity for SuperKEKB," Proc. PAC'05, Knoxville (2005).